Formulation induces direct DNA UV-A photooxidation. Part II. Pro-oxidant effect of formulated Vitamin E via generation of singlet oxygen

Johanne Teychené, Dalina Didacus-Prins, Nadia Chouini-Lalanne, Christophe Dejugnat, Valérie Sartor

To cite this version:

Johanne Teychené, Dalina Didacus-Prins, Nadia Chouini-Lalanne, Christophe Dejugnat, Valérie Sartor. Formulation induces direct DNA UV-A photooxidation. Part II. Pro-oxidant effect of formulated Vitamin E via generation of singlet oxygen. Journal of Molecular Liquids, 2020, 316, pp.113818. 10.1016/j.molliq.2020.113818. hal-02916908

HAL Id: hal-02916908
https://hal.science/hal-02916908v1

Submitted on 6 Nov 2020

Formulation induces Direct DNA UV-A photooxidation. Part II. Pro-oxidant effect of formulated Vitamin E via generation of singlet oxygen

Johanne Teychené, Dalina Didacus-Prins, Nadia Chouini-Lalanne, Christophe Déjugnat, Valérie Sartor**

HIGHLIGHTS

- Cetyltriethylammonium bromide (CTEAB) and Vitamin E self-assemble in TRIS/HCl buffer solutions into nanoemulsion composed of CTEAB micelles (that can incorporate Vitamin E) as well as larger Vitamin E droplets.
- CTEAB-Vitamin E nanoemulsion interacts with plasmid DNA pBR322 and the gradual DNA compaction followed by gradual DNA decompaction for increasing CTEAB-Vitamin E amounts have been highlighted.
- UVA irradiation induces photooxidation of DNA on the formulated CTEAB-Vitamin E-DNA lipoplex and underlines the pro-oxidant role of the Vitamin E in this self-assembled system.

Formulation induces Direct DNA UV-A photooxidation. Part II. Pro-oxidant effect of formulated Vitamin E *via* generation of singlet oxygen

Johanne Teychené[1], Dalina Didacus-Prins[2], Nadia Chouini-Lalanne[2], Christophe Déjugnat[2], Valérie Sartor[2]**

1- TBI, Université de Toulouse, INSA, INRA, CNRS, Toulouse, France

2- Laboratoire des IMRCP, Université de Toulouse, CNRS UMR 5623, Université Toulouse III - Paul Sabatier

Abstract

The study focuses on the photosensitization of DNA in nanoemulsion-type systems containing Vitamin E under UVA radiation. Cetyltriethylammonium bromide (CTEAB) surfactant was first combined with Vitamin E to form a CTEAB-Vitamin E nanoemulsion to complex the plasmid pBR322, in TRIS/HCl buffer. The self-organization properties of the CTEAB-Vitamin E system were studied by complementary physico-chemical characterizations (tensiometry, pyrene fluorimetry and scattering experiments). It formed a nanoemulsion composed of CTEAB micelles (that can incorporate Vitamin

E) as well as larger Vitamin E droplets. This nanoemulsion was then contacted with DNA and the resulting formulated CTEAB-Vitamin E-DNA lipoplex was irradiated under UVA radiation ($\lambda \geq 335$ nm). The presence of Vitamin E generated a significant enhancement of the DNA photodamage as shown by agarose gel electrophoresis and quantified by photodensitometry. It underlines the pro-oxidant role of the Vitamin E in this self-assembled system. A mechanistic study based on the use of specific scavengers reveals that the singlet oxygen is responsible for the UVA DNA photooxidation in the CTEAB-Vitamin E-DNA lipoplex.

Keywords

Surfactant; self-assembly; DNA; UVA photosensitization; Vitamin E

1. Introduction

The development of chemical models capable of preventing highly mutagenic lesions induced by UV radiation is a major therapeutic challenge in the field of oncology and more particularly in the field of prevention. The design of alternative systems to protect people from these lesions is therefore a real challenge.

Reactive oxygen species (ROS) are permanently generated, transformed, and consumed in all living organisms due to metabolic and biochemical reactions as well as external factors. These species are responsible, directly or indirectly, for many oxidative damage at the molecular level that threaten the stability and integrity of DNA, cell membranes, and proteins. In the cell, antioxidant systems prevent damage caused by free radicals, including alpha-tocopherol, which commonly refers to Vitamin E (VitE) (Fig 1). Thanks to its antioxidant properties against ROS, VitE offers a protective effect to the skin against cell membrane lipid peroxidation and DNA oxidative damage, safeguarding the stability and the integrity of the cell. Therefore, the administration of VitE in many pharmaceutical, cosmetic, and food products[1,2] has been a strategy to decrease DNA damage and ultimately to prevent skin disorders.[3,4] However, prooxidant and antioxidant properties of VitE are still not clearly understood. For instance, Dad and al. [5] evidenced that alpha-tocopherol is able to generate singlet oxygen, a highly reactive oxygen species responsible in particular for oxidative damage to DNA, when excited in the UVB region at 308 nm. Another work reports the production of endogenous photosensitizer for UVA radiation after exposure of VitE to UVB.[6] Nocentiny and al.[7] provided evidence of singlet oxygen production during the photolysis of VitE under UVB. These works call into question the VitE functional efficacy as antioxidant.

VitE is a lipid-soluble biological organic compound present in mammalian skin and located in cell membranes (Fig.1). Its use is still limited because of its poor water solubility. To overcome this problem, new stable formulations of Vit E have been developed to ensure its encapsulation and transport.[4,8] Among them, micellar solutions are used as delivery systems for active ingredients. Indeed, the solubilization of the active substances into micro- and nanoemulsion-type systems is an efficient way to obtain small sized self-assembled aggregates, allowing the transport of the active compound.[9,10] However, the efficacy of formulated antioxidants depends on the properties of the system: type of emulsion, type of oil, type of surfactant.[8] These various studies raise the question of the stability of VitE in nanoemulsion-type systems under UVA radiation.

In this context, the purpose of this work is to extend the study of the photosensitization of singlet oxygen by VitE under UVA radiation in self-assembled systems, and to study the impact it could have on DNA duplex.

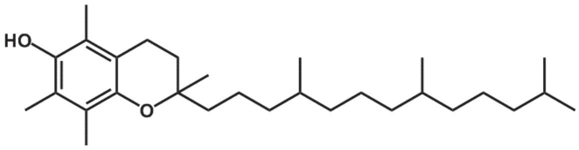

VitE

Fig.1. *Molecular structure of α–tocopherol (VitE)*

The self-organization properties of cetyltriethylammonium bromide (CTEAB) and the CTEAB-DNA lipoplex in TRIS/HCl buffer have been described in our previous paper.[11] Results showed that CTEAB can be used to formulate DNA and pointed out also the effects of compaction on DNA photodamage under UVA radiation which induce the self-photosensibilisation of DNA.

In the present study, we developed a cationic nanoemulsion system including CTEAB to deliver the active principle VitE as an integral part of the emulsion. More precisely, we used VitE simultaneously as oil phase and as active ingredient, a kind of 2-in-1 self-formulated VitE.

In a first part, we present the self-organization properties of CTEAB and VitE in the buffer solution used as solvent for DNA. The determination of the critical aggregation concentration (CAC) (by tensiometry and pyrene fluorimetry) and the depiction of the self-assembled aggregates (by scattering experiments) will be shown. Then, the interactions between the CTEAB-VitE formulation – later called as {CTEAB@VitE} – and DNA will be characterized to check that {CTEAB@VitE} can be used to formulate DNA (by tensiometry and pyrene fluorimetry). Finally, the effects of UVA irradiation on these formulations will be investigated by agarose gel electrophoresis. Results will show that the formulations can affect the integrity of DNA due to DNA photooxidative damage. The mechanistic interpretation of the results will be highlighted by the use of peculiar scavengers.

2. Materials and methods

2.1 Materials

Cetyltriethylammonium bromide (CTEAB) was synthesized as described in our previous article.[11] α-tocopherol (Vitamine E or VitE) in racemic form, heparin sodium salt, and sodium azide (NaN_3) were purchased from Alfa Aesar. Agarose and tert-butanol (*ᵗ*BuOH) were obtained from Sigma-Aldrich. Pyrene was purchased from Acros Organics and Ethidium bromide (EB) from Pharmacia Biotech PLUSONE as a 10 mg·mL^{-1} aqueous solution. Eurisotop furnished D_2O and BioLabs the T4 endonuclease V (pyrimidine dimer glycosylase) enzyme. The reagents were used as received. Tris(hydroxymethyl)aminomethane (TRIS) and supercoiled plasmid DNA (Form I) pBR322 (4361 base pairs) were purchased from Thermo Fisher Scientific. The DNA was used after dilution in a 20 mM TRIS/HCl buffer (pH = 7.4) to obtain a stock solution at [DNA-PO_4^-] = 4.5×10^{-4} mol·L^{-1}. All DNA concentrations indicated in the manuscript are in mol phosphate·L^{-1}.

Water used in all experiments was produced by a two-stage Milli-Q filtration system from Millipore and had a resistivity higher than 18.2 MΩ·cm.

2.2 {CTEAB-VitE} preparation

Colloidal dispersions {CTEAB-VitE} were formulated using a technique based on the preparation of liposomes by the thin film hydration method.[12,13] Preparations were obtained by mixing CTEAB and VitE, both dissolved in ethanol. The solution was then evaporated to dryness using a rotary evaporator and the film thus obtained was re-dispersed in a 20 mM TRIS/HCl solution (pH = 7.4). The final CTEAB concentration was 8.33×10^{-4} mol·L^{-1}, corresponding to more than 5 times the CMC value of CTEAB in TRIS/HCl (1.5×10^{-4} mol·L^{-1}).[11] The final concentration of VitE was 3.58×10^{-4} mol·L^{-1}

corresponding to a VitE / CTEAB concentration ratio of 0.43. This ratio corresponded to the maximal solubility of formulated VitE in the aqueous solution.

2.3 Surface tension measurements

Surface tension measurements were performed using a Krüss EasyDyne tensiometer using the Wilhelmy plate method. Temperatures were maintained at 25 °C (± 0.1 °C) by circulating thermostated water through a jacketed vessel containing the solution. For each experiment, surface tension was measured three times (each time ten readings were performed and averaged) after an equilibration time of 30 minutes.

2.4 Fluorescence measurements

A stock solution of pyrene (10^{-4} mol·L^{-1}), was prepared in methanol and stored at 4 °C. The solutions for fluorescence probing studies were prepared by adding 1 µL of this pyrene stock solution to 399 µL of the sample solution. Final concentration of pyrene was 2.5×10^{-7} mol·L^{-1}, while the amount of methanol remained very low (0.25 % vol.). Fluorescence measurements were performed using a Fluorolog Horiba spectrofluorimeter, with a thermostated cuvette holder at 25 ± 0.1 °C. Excitation wavelength was 335 nm, and the fluorescence emission was recorded from 350 to 500 nm.

2.5 Multi-angle light scattering experiments

The measurements were performed on a 3D LS Spectrometer from LS Instruments (Fribourg, Switzerland) equipped with a 100 mW high performance DPPS Laser (Cobolt) operating at $\lambda = 660$ nm, a two-channel multiple tau correlator (auto and cross correlation, 1088 real time channels), a 3D cross-correlation module, a variable-angle detection system, two high sensitivity APD detectors, an automated laser attenuation system combined with on-line laser intensity measurement, a temperature controllable sample chamber with index matching vat, and an external circulator for temperature control (Julabo CF31).

Before analysis, samples (1.1 mL) were placed into cylindrical scattering cells (10 mm diameter), either directly or after filtration through hydrophilic PTFE filters (450 or 200 nm porosity), as specified in the text.

Measurements were performed at 25°C for scattering angles θ ranging from 12° to 150°, corresponding to scattering wave vectors q in the range 2.7×10^{-4}-2.4×10^{-3} Å^{-1}. As samples produced multiple scattering, the 3D cross-correlation configuration was required.[14]

At each angle, 3 to 10 measurements were carried out and later averaged after having discarded eventual meaningless correlograms. Analysis of both dynamic- and static light scattering measurements were performed using the home-made MULTI-STORMS software developed by Dr. C. Mingotaud (see *Supporting Information*).

2.6 Small-Angle x-ray Scattering (SAXS) experiments

SAXS measurements were conducted on a Xeus 2.0 SAXS beamline for laboratory from Xenocs (FERMAT federation, Toulouse), with an internal copper source producing 8 keV x-rays (wavelength = 1.54 Å). Signals were recorded using a Pilatus 1M pixel detector from Dectris. The sample-to-detector distance was varied from 387.5 mm to 1687.5 mm so that the covered q range was $0.0042 < q < 0.7$ Å^{-1}. Two scans of 120 min were recorded at each distance and averaged. The observed intensity I(q) was corrected for transmission, solvent, and detector response. Absolute intensity I(q) (cm^{-1}) was obtained after standard normalization. The analysis of the I(q) profile was realized using the SasView software (http://www.sasview.org/), version 4.2.2.

2.7 Irradiation experiments

DNA irradiation was made with a Mercury Xenon lamp (Oriel instruments, 500W) equipped with a long pass filter λ ≥ 335nm (Newport 20CGA-335 GC505) at 20°C. The irradiated and non-irradiated sample volumes were 100 µL. The final concentrations in TRIS/HCl buffer (20 mM, pH=7.4) were 9×10^{-5} mol phosphate·L^{-1} for the plasmid DNA pBR322, 5×10^{-4} mol·L^{-1} for CTEAB, 2.15×10^{-4} mol·L^{-1} for VitE, 200×10^{-3} mol·L^{-1} for NaN_3, and 4% v/v for *t*BuOH. Each experiment was at least triplicated.

2.8 Agarose gel electrophoresis

2.8.1 Sample preparation

50 µL of the sample solution were used in the T4 endonuclease V experiments. It consists to add 10 µL of T4 endonuclease V (10000 U/ml) to 50 µL of DNA containing sample and to incubate the solution 30 min at 37°C. 5 µL of bromophenol blue solution and 10 µL of Heparin 20% (w/w in TRIS/ HCl buffer (20 mM, pH= 7.4) are then further added.

For the samples without T4 endonuclease V treatment, 5 µL of bromophenol blue solution, 10 µL of Heparin 20% (w/w in TRIS/ HCl buffer), and 10 µL of 20 mM TRIS/HCl (pH= 7.4) were added to 50 µL of formulated DNA.

2.8.2 Electrophoresis and photodensitometry

An aliquot of 40 µL of each sample was deposited into 0.8% agarose gel containing 0.02 % of Ethidium bromide. Electrophoresis migration was carried out for 4 hours under a constant electric field of 80 V.

Single strand breaks (SSB) were quantified by photodensitometry using the ImageJ software. To correct the lower efficiency of Ethidium bromide binding to Form I DNA with respect to Form II, a coefficient of 1.66 was used.[15]

3. Results and discussion

3.1. Self-organization of CTEAB and VitE in TRIS/HCl buffer

The critical aggregation concentration (CAC) measurement has been carried out by two complementary methods (tensiometry and fluorimetry) in {CTEAB@VitE} mixtures.

Surface tension as a function of CTEAB concentration in presence of Vitamin E in TRIS/HCl buffer solution is shown in Fig. 2, along with the curve of pure CTEAB for comparison.

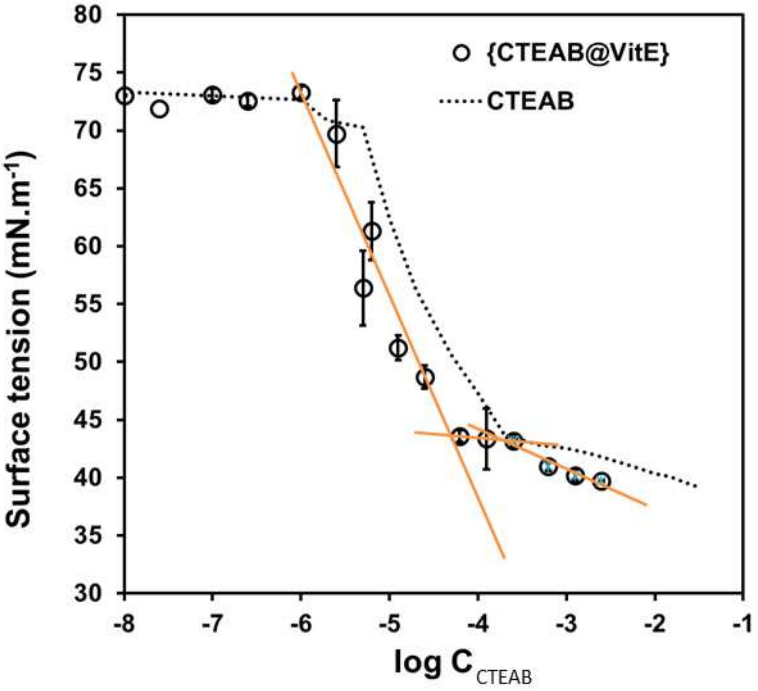

Fig. 2. *Surface tension as a function of surfactant concentration in 20 mM TRIS/HCl buffer, pH = 7.4, 25°C. Open circles:* {CTEAB@VitE} *mixture. Dotted line: pure CTEAB.*[11]

In the dilute regime, the surface tension value is equal to the one of water and then it decreases as the concentration of surfactant increases to finally reach a plateau. The surface tension curve of {CTEAB@VitE} mixture exhibits two break points. The first one corresponds to the CAC, from which the {CTEAB@VitE} complex is formed. The second one is the CMC of free remaining CTEAB. By this technique, the CAC of {CTEAB@VitE} and the CMC of CTEAB in {CTEAB@VitE} mixture are found to be 4.8×10^{-5} mol·L^{-1} and 2×10^{-4} mol·L^{-1} respectively. After the {CTEAB@VitE} complex is formed, at a CTEAB concentration of 4.8×10^{-5} mol·L^{-1}, the micellization of free remaining CTEAB in the mixture occurs at a CTEAB concentration of 2×10^{-4} mol·L^{-1}. Hence, 4.8×10^{-5} mol·L^{-1} corresponds to the difference between 2×10^{-4} mol·L^{-1} and 1.5×10^{-4} mol·L^{-1}. That means that the CMC of CTEAB in the {CTEAB@VitE} mixture or in pure form remains the same (1.5×10^{-4} mol·L^{-1}).

The surface tension in the mixture is lower than that of the pure CTEAB, indicating the formation of a cooperative complex between CTEAB and VitE. The later attracts more surfactant at the air/solution interface.

The aggregation properties studies of {CTEAB@VitE} in TRIS/HCl buffer have also been carried out by pyrene fluorescence measurements. The I_1/I_3 pyrene fluorescence ratio (I_1 at 383 nm and I_3 at 393 nm respectively) are reported in Fig. 3 as a function of CTEAB concentration for {CTEAB@VitE} in TRIS/HCl buffer. For comparison, the I_1/I_3 pyrene fluorescence variation is also represented for CTEAB in buffer solution. To determinate the CAC, results have been adjusted by a sigmoidal Boltzmann function.[16]

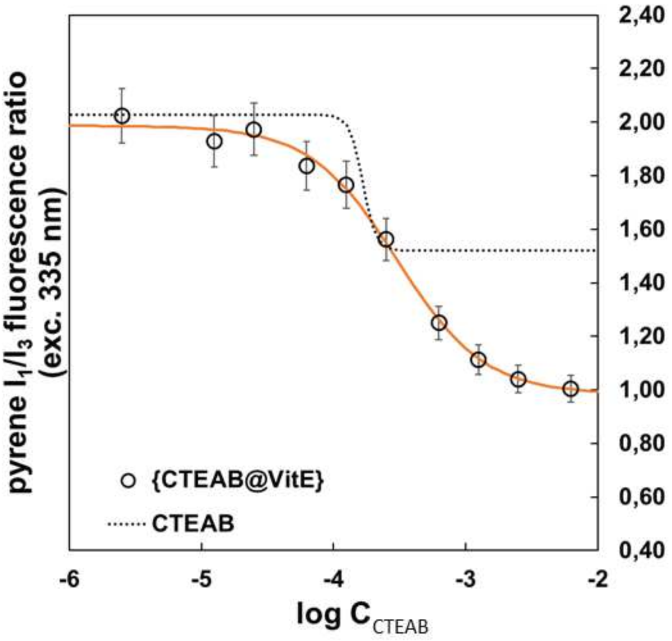

Fig. 3. *Pyrene I_1/I_3 fluorescence ratio as a function of surfactant concentration in 20 mM TRIS/HCl buffer, pH = 7.4, 25°C (excitation 335 nm). Open circles: {CTEAB@VitE} mixture. Dotted line: CTEAB.*[11]

The I_1/I_3 ratio in the {CTEAB@VitE} system changes sharply around the CAC, *i.e.* about 2.5×10^{-4} mol·L^{-1}. This value is quite close to the 2×10^{-4} mol·L^{-1} value obtained by surface tension measurements. The I_1/I_3 ratio of the pyrene spectra, for high CTEAB concentrations, is directly related to the apparent dielectric constant of the probe environment in the micelles; both values are reported in Table 1.[17]

VitE / CTEAB concentration ratio	I_1/I_3 ratio (for high CTEAB concentrations)	Apparent dielectric constant ε
0	1.5	54.5
0.43	1.0	19.2

Table 1. *Ratio of the first and third vibronic peak of pyrene (I_1/I_3) in micelles as a function of Vitamin E / CTEAB concentration ratio in 20 mM TRIS/HCl buffer, pH = 7.4, 25 °C. Apparent dielectric constant ε calculated from the correlation $I_1/I_3 = 0.0145\ \varepsilon + 0.7022$.*[17]

The dielectric constant value in {CTEAB@VitE} is 19.2, which is much lower than the value obtained in the pure CTEAB solution (54.5). In {CTEAB@VitE}, the probe microenvironment is less polar than in pure CTEAB solution, meaning that the amount of water in the micelles decreases as the VitE concentration increases. Therefore, the addition of VitE promotes the formation of hydrophobic domains in this system.

In summary, close CMC values are obtained whether or not the presence of VitE in solution. This might suggest that VitE has only a slight impact on the self-assembly of CTEAB. However, the presence of VitE creates a less polar environment than in pure surfactant micelles, meaning that water has been ejected from the micelles. Thus, this seems to indicate that the water that hydrated the CTEAB head groups was ejected and replaced by VitE, leading to the formation of mixed CTEAB/VitE micelles.

Further characterizations of the aggregates were conducted by the means of scattering experiments (light and x-rays).

Multi-angle dynamic- and static light scattering (MADLS and MASLS, respectively) were first performed on the {CTEAB@VitE} system which will be later put in contact with DNA (*i.e.* [CTEAB] = 8.33×10^{-4} mol·L^{-1} and [VitE]/[CTEAB] = 0.43). The sample was slightly opalescent and preliminary measurements indicated that multiple scattering occurred. For this reason, the 3D cross-correlation technique[14] was used to overcome this problem by discarding the multiple scattering contribution from the total scattered light.

In light scattering, the scattering wave vector q is defined as a function of the scattering angle θ as described in (1).

$$q = \frac{4\pi n \sin(\theta/2)}{\lambda} \tag{1}$$

where n is the refractive index of the solvent and λ the wavelength of the incident light.

MADLS measurements afford the autocorrelation function of the scattered light intensity, normalized over time. A mathematical adjustment then gives access to the decay rate Γ which is related to the translational diffusion coefficient D_0 ($\Gamma = D_0 \cdot q^2$ for a monodisperse system with only translational diffusion). Finally, the hydrodynamic radius R_h is then given by the Stokes-Einstein relationship (2):

$$R_h = \frac{kT}{6\pi\eta D_0} \tag{2}$$

where k is the Boltzmann constant, T the absolute temperature, and η the solvent viscosity.

The experimental correlation functions (shown in the *Supporting Information, Figure S1*) could be well fitted in the whole range of wave vectors by using a 2nd order Cumulant analysis, which afforded the corresponding decay rates. Plot of the first decay rate Γ as a function of q^2 is presented in Fig. 4A. Obviously $\Gamma = f(q^2)$ was not a linear function, indicating that the relaxation motion recorded by DLS was not solely the translational diffusion coefficient of the scattering particles. It could rather include additional internal motions (such as local rotations for example), probing the particles dynamics at a length scale smaller than their hydrodynamic radius.[18] Even at very low q values, data could only roughly be fitted by a line passing through the origin, whose slope afforded an estimation of an apparent lateral diffusion coefficient $D_{app} \approx 4\times10^5$ $nm^2 \cdot s^{-1}$, corresponding to an apparent hydrodynamic radius $R_{h,app} \approx 600$ nm. At higher q values, the q^n dependence of Γ (n > 2) could be well described by plotting log Γ = f(log q), showing a linear dependence with slope n = 2.94 (Fig. 4B). This value is very close to the asymptotic Zimm limit (n = 3),[19] which is reached in the case of polymer chains or fractal aggregates under strong hydrodynamic interactions.[20–22]

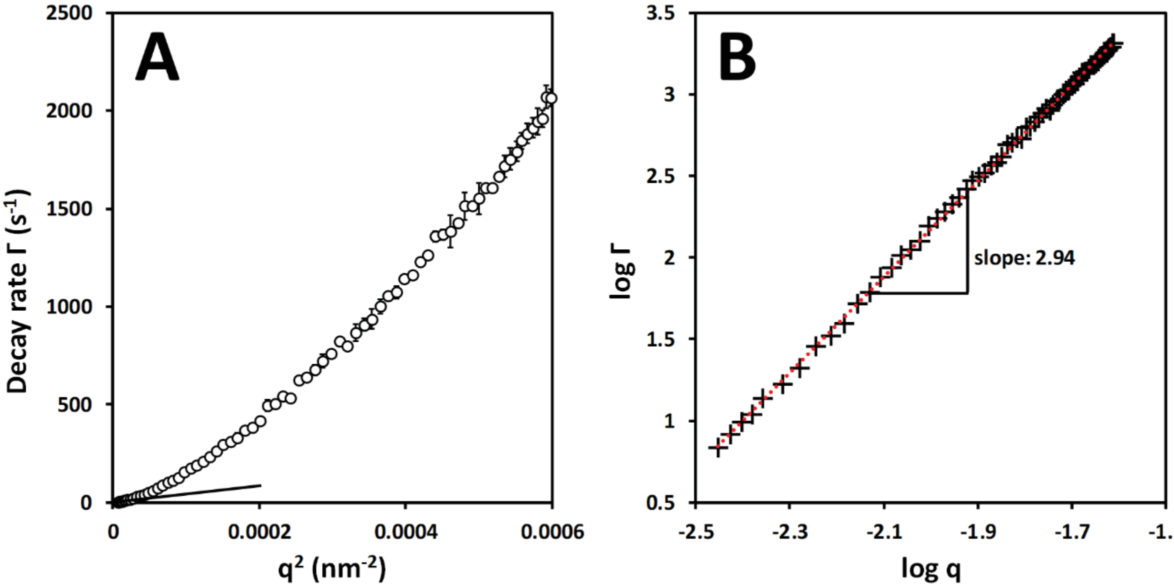

Fig. 4. *(A): decay rate* Γ *(*s^{-1}*) as determined from a 2nd order Cumulant analysis, plotted as a function of* q^2 *from MADLS measurements of {CTEAB@VitE}; open circles are the experimental data and the line is the linear fit at very low q values. (B): plot of log* Γ *as a function of log q showing a linear dependence with a slope very close to 3.*

As no polymer was present in the {CTEAB@VitE} system, we could hypothesis the presence of a fractal association or a network of strongly (attractive) interacting particles formed by irreversible diffusion-limited aggregation.[23] Therefore, the observed high value of R_h could correspond to long-range assembled structures rather than to elementary aggregates. To get further insights on this self-assembled system, we performed MADLS measurements on samples filtered at 450 nm and 200 nm respectively. Data treatments showed that the slopes in the log Γ = f(log q) curves decreased and got closer to 2. At very low q values, the $\Gamma = f(q^2)$ variation was even linear, allowing more accurate determination of translational diffusion coefficients and hydrodynamic radii, which were found to tend to R_h = 120 nm (Figures S3, S5, *Supporting Information*). Complementary multi-angle static light scattering (MASLS) characterizations were performed on these samples from 12° to 150° ($q = 2.6\times10^{-4}$-2.4×10^{-3} Å^{-1}). Absolute scattered intensities I(q) expressed as Rayleigh ratios (see *Supporting Information*) are reported in Figure 5.

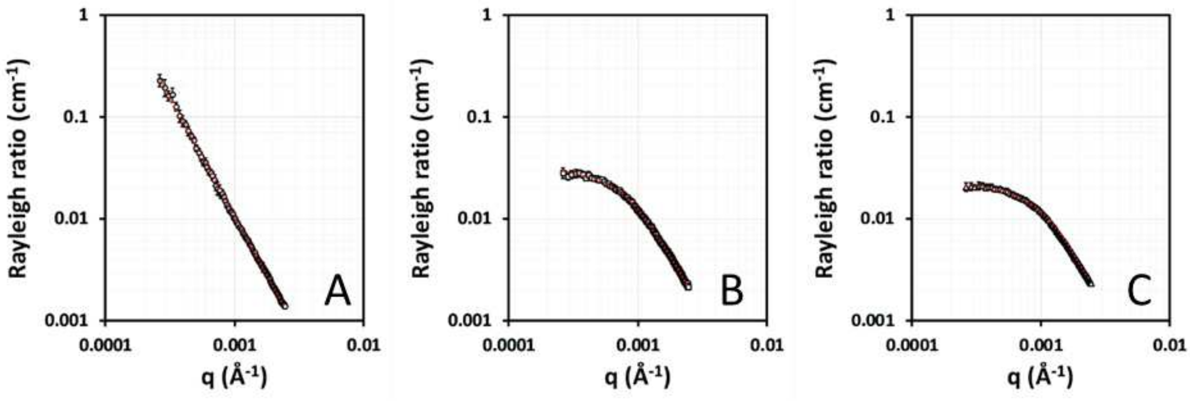

Fig. 5. *Absolute scattered light intensities as obtained by MASLS measurements for native {CTEAB@VitE} (A) or after filtrations at 450 nm (B) or 200 nm (C). Red dotted lines are mathematical adjustments.*

Regarding the native sample (unfiltered) (Fig. 5A), the scattering profile showed a $q^{-2.3}$ regular variation and could be well adjusted using a fractal model. Indeed, the fractal dimension 2.3 determined from the SLS curve corresponds to a compact fractal system.[24–26] Upon filtration, the scattering profiles changed and exhibited a plateau at low q values followed by a q^{-2} variation at higher q values (Fig. 5B and 5C). This suggests that these measurements are better describing individual particles (or primary aggregates) forming the fractal network. General Guinier-Porod fits afforded a radius of gyration R_g = 115 nm, while the scattering profile of the sample filtered at 200 nm could also be fairly well adjusted using a spherical form factor (R = 143 nm) associated to a sticky hard sphere structure factor (see models descriptions in the *Supporting Information*). Altogether, these light scattering experiments support the hypothesis of a nanoemulsion system where spherical VitE droplets exhibit strong attractive interactions that lead to a fractal organization at higher scale.

Complementary techniques were then used to get further information about this system, namely small-angle x-ray scattering (SAXS). Preliminary experiments indicated that the sample was not concentrated enough to get reliable results. We then had to consider a much more concentrated sample (30 times more concentrated than the initial system). Before SAXS analysis, we first checked by light scattering that the concentrated sample could be representative of the initial one, as not dramatic differences could be evidenced between the two samples by MADLS and MASLS, even upon filtration (Fig. S6, *Supporting Information*). SAXS measurements are reported in Fig. 6A together with MASLS data recorded on the same sample. The overall spectrum could then be adjusted using a multi-contribution function, including a fractal system and two distinct populations of spherical objects with two different sizes (See *Supporting Information*). The overall description of the system then leads to a fractal network of large oil VitE droplets together with very small CTEAB empty micelles (R = 1.5 nm) but also swollen CTEAB micelles containing VitE in their core (R=6.5 nm). This multi-scale description is in accordance to what reported in literature in the case of oil-in-water nanoemulsions obtained by a low-energy method such as the solvent inversion technique,[9,27] and is depicted in Figure 6B.

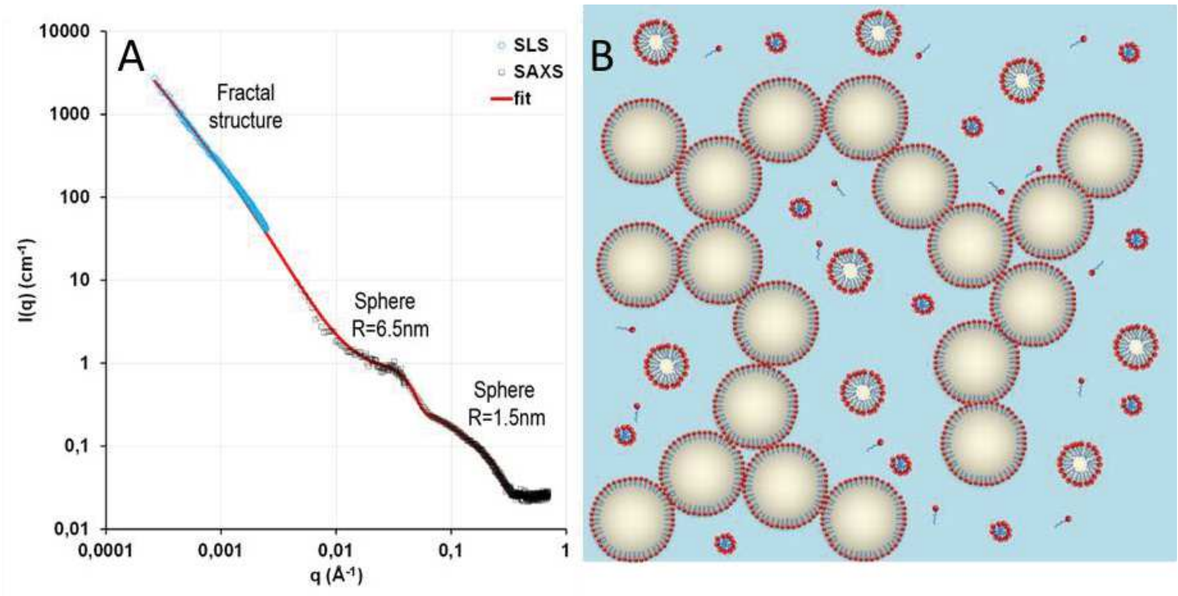

Fig. 6. *(A): Combination of MASLS (blue open circles) and SAXS (black open squares) measurements of the {CTEAB@VitE} nanoemulsion, and the corresponding overall fit (red curve) indicating the presence of different aggregates. (B): Schematic representation of the nanoemulsion formed by the {CTEAB@VitE} system, as deduced from scattering experiments.*

3.2. Interaction between DNA and {CTEAB@VitE} aggregates

The use of {CTEAB@VitE} aggregates as non-viral vectors for DNA is of concern because of its great potential in gene therapy for the development of protective (antioxidant) formulations. In this context, different techniques were carried out to study the interactions between the {CTEAB@VitE} aggregates and the model plasmid DNA pBR322.

The effect of DNA on the {CTEAB@VitE} aggregates was investigated using tensiometry (Fig. 7A) and fluorimetry (Fig. 7B) for increasing CTEAB concentrations (VitE / CTEAB concentration ratio = 0.43).

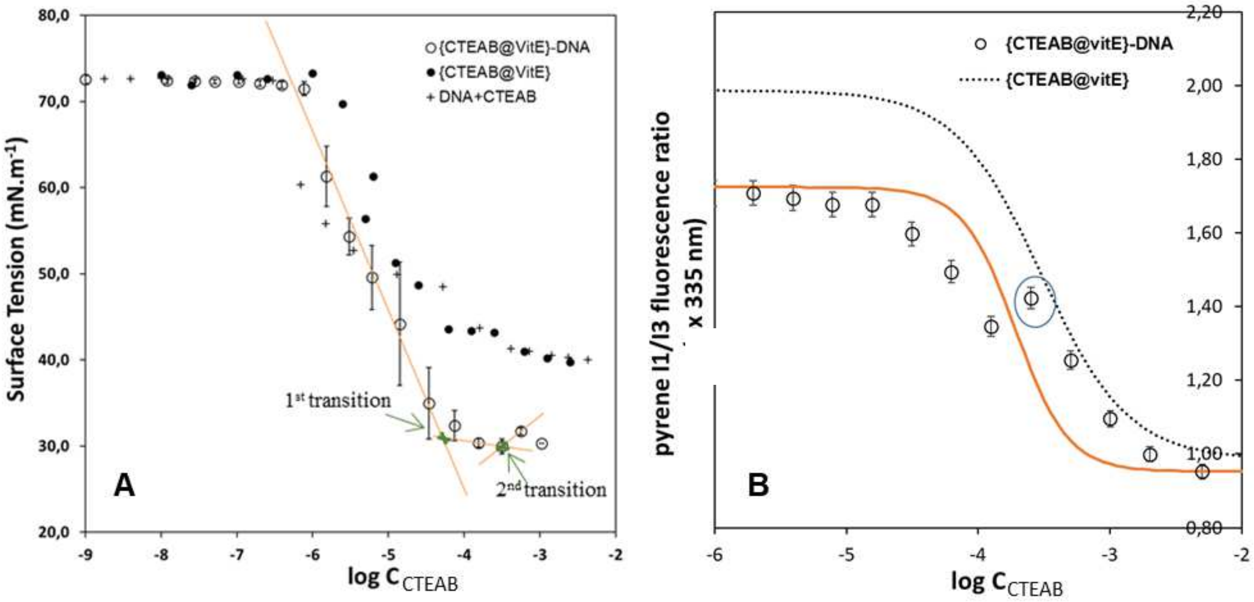

Fig. 7. *(A): Surface tension measurements of DNA solutions as a function of CTEAB concentration in {CTEAB@VitE}, in 20 mM TRIS/HCl buffer, pH = 7.4, 25 °C ([VitE]/[CTEAB] = 0.43, [DNA-PO$_4^-$] = 9.10^{-5} mol·L^{-1}). Open circles:* {CTEAB@VitE} – DNA *mixture. Filled circle:* {CTEAB@VitE}–DNA *mixture. Cross: DNA+CTEAB mixture.*[11]

(B): Pyrene I$_1$/I$_3$ fluorescence ratio in aqueous solution of DNA as a function of CTEAB concentration in {CTEAB@VitE}, in 20 mM TRIS/HCl buffer, pH = 7.4, 25 °C ([VitE]/[CTEAB] = 0.43, [DNA-PO$_4^-$] = 9.10^{-5} mol·L^{-1}). Empty circles: {CTEAB@VitE} – DNA *mixture. Dotted line: {CTEAB@VitE} mixture.*

The surface tension curve of {CTEAB@VitE}-DNA lipoplex (Fig. 7A) is underneath the two other curves (DNA + CTEAB [11] and {CTEAB@VitE}), suggesting that the complexation between CTEAB, VitE, and DNA has a strong effect on the surface tension. The surface tension of the {CTEAB@VitE}-DNA solution sharply decreases until a first transition appears at a CTEAB concentration of 5.2×10^{-5} mol·L^{-1} (log C=-4.2), corresponding to the CAC obtained in {CTEAB@VitE} nanoemulsion (4.8×10^{-5} mol·L^{-1}). Interestingly, further addition {CTEAB@VitE} between CTEAB concentration of 5.2×10^{-5} mol·L^{-1} (log C=-4.2)) and 3.2×10^{-4} mol·L^{-1} (log C=-3.5), results in a constant surface tension, suggesting a synergistic aggregation between DNA and {CTEAB@VitE}. [28] Then, the surface tension seems to increase slightly and shows a second transition at 3.2×10^{-4} mol·L^{-1} (log C=-3.5), that might correspond to the free DNA depletion from the air/water interface. [28]

To complement these results, pyrene I_1/I_3 emission fluorescence ratio as a function of the CTEAB concentration is presented in Fig. 7B in {CTEAB@VitE}-DNA lipoplex. A roughly sigmoidal shape related to a phase transition and a formation of hydrophobic domains is observed. For low CTEAB concentrations, the I_1/I_3 ratio was found to be 1.70 instead of 2.00 in the {CTEAB@VitE} system. This decrease means that pyrene has found to locate in more hydrophobic places. Indeed, different works reported pyrene can interact via partial intercalation with DNA. [29] Below the phase transition, the increase in {CTEAB@VitE} concentration is accompanied by an increase in turbidity, observed macroscopically. Previous work[11] has shown that the increase in turbidity could be associated with strong electrostatic interactions between the DNA and the surfactant, suggesting a gradual compaction of DNA. Progressive compaction refers to a state where individual {CTEAB@vitE} aggregates decorate the DNA and form hydrophobic domains on the DNA strand. The sharp I_1/I_3 ratio decrease can be associated with the critical aggregation concentration that occurs for a CTEAB concentration of 2.5×10^{-4} mol·L^{-1} (log C=-3.6) and which corresponded to the 2nd transition observed by tensiometry (Fig. 7A). This CAC evidences again the synergic cooperation between {CTEAB@VitE} and DNA. This remarkable point (Fig.7B, circled point), corresponding to an increase in I_1/I_3 ratio, also matches with a turn from a turbid solution to a limpid solution. This concentration value is in line with the transition observed in surface tension measurements (3.2×10^{-4} mol·L^{-1}). The transition from a turbid to a limpid solution could indicate the formation of another type of {CTEAB@VitE}–DNA complex due to a large excess of CTEAB. Notably, it could correspond to a DNA decompaction process, as already reported in the literature for excess amount of cationic surfactant.[30–32] This transition in {CTEAB@VitE}–DNA system appears at much lower CTEAB concentration that the one reported in CTEAB-DNA system[11] (between 20 and 30 $\times 10^{-4}$ mol·L^{-1}). The presence of vitamin E in the complex seems to promote the DNA decompaction.

The I_1/I_3 ratio value of 0.96, obtained for high {CTEAB@VitE} concentrations in {CTEAB@VitE}-DNA system, corresponds to a micellar dielectric constant of 17, meaning that the pyrene environment is apolar. This dielectric constant value is identical as the one obtained for the {CTEAB@VitE} formulation, suggesting that the presence of DNA does not affect the local micropolarity of pyrene environment, which remains in both systems hydrophobic.

3.3. **Photochemistry**

Photostability of non-viral vectors is an important concern regarding their topical uses. The {CTEAB@VitE}-DNA lipoplex was formed with a DNA model, the plasmid pBR322, and the nanoemulsion {CTEAB@VitE} described above. Its photostability under UVA irradiation (λ ≥ 335 nm) was studied by agarose gel electrophoresis. Indeed, photodegradation of plasmid pBR322 in supercoiled form (or Form I) induces the formation of single strand breaks (SSB) leading to its relaxed circular form (or Form II). This results in two distinct bands on the agarose gel electrophoresis, noted as I (Form I) and II (Form II) on the gel pictures. In addition, each band can be quantified by photodensitometry.

The solutions were irradiated one minute. With this time of irradiation, and in presence of {CTEAB@VitE}-DNA complex, DNA photodamage are well quantified while no overbreaks are observed. (Fig. 8A, lane 6*) UVA irradiation of the {CTEAB@VitE}-DNA lipoplex (Fig. 8A, lane 6*) induces around a threefold increase of the SSB ratio (Fig. 8B) compared to CTEAB-DNA complex (Fig. 8A, lane 5*). The presence of Vitamin E on the lipoplex generates a significant enhancement of the DNA photodamage. As the formation of singular oxygen by CTEAB-DNA complex by a Triplet-Triplet energy transfer mechanism has been previously reported,[11] we have investigated the formation of damage to DNA that may be caused by such a mechanism, namely the formation of CPD and the formation of singular oxygen to determine the mechanism involved in this photodegradation. First, the samples were treated by a phage T4 endonuclease V enzyme (T4), a DNA enzyme repair that cleaves double-strand DNA at cyclobutane pyrimidine dimer (CPD), leading to single strand breaks by a two-step mechanism. In this study, if CPD is formed by photosensitization and the plasmid pBR322 treated with T4, single strand break will be made and the Form II of the plasmid will appear on the electrophorese agarose gel. T4 treatment on non-irradiated plasmid pBR322 reveals the presence of abasic lesions by AP-lyase activity of the T4 (Fig. 8A, lane 7 and Fig. 8B). Without irradiation, in presence of CTEAB or {CTEAB@VitE} and with T4 treatment, the SSB ratio decreases dramatically (lanes 8 and 9 respectively), as already shown for CTEAB-DNA lipoplex.[11] The hypothesis was an enzyme quenching in presence of the CTEAB or the non-access to the DNA double strand to the enzyme because of its compaction. It was also previously observed that after 10 min irradiation, the T4 treatment revealed again the DNA photodamage.[11] In these experiments and for a lower time of irradiation (1 min), the photooxidative damage of the plasmid induced by the CTEAB alone are limited (lane 5*). That's what the SSB ratio observed should be due, only to abasic lesions already present in native DNA, and to the CPD formed under irradiation. After T4 treatment of the sample (lane 11*), the SSB ratio becomes again equivalent to the SSB ratio for DNA alone (lane 10*) and the native DNA abasic site level is recovered and no increase of the SSB ratio is observed in presence of CTEAB and one minute of irradiation, compared to DNA alone (Fig. 8B). No CPD are formed and the T4 enzyme works again if the sample is irradiated. The small amount of damage formed by the irradiation seems enough to induce some modification on the DNA compaction and to allow recovering the enzymatic activity of the T4 endonuclease V.

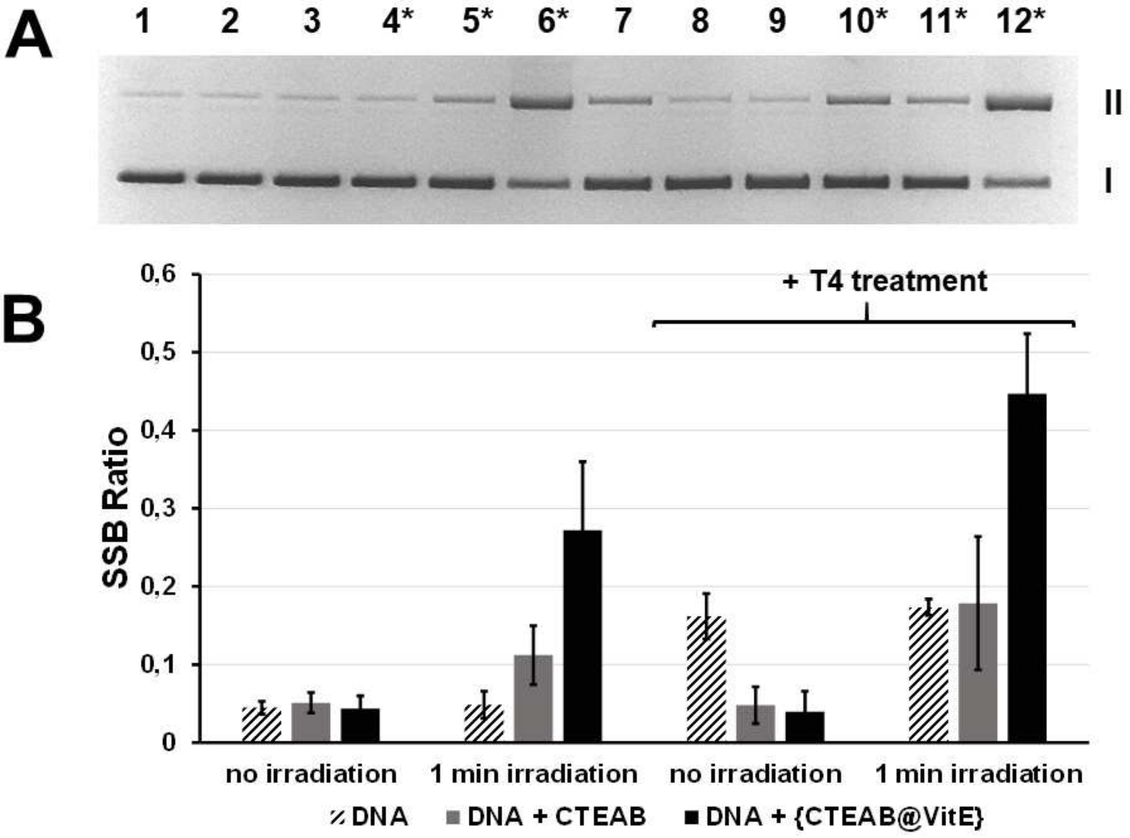

Fig. 8. *DNA cleavage for 1 min of irradiation at λ ≥ 335nm and 20°C with CTEAB (5×10^{-4} mol·L^{-1}) or {CTEAB@VitE} after or not phage T4 endonuclease V treatment (T4) (* indicates the irradiated samples). A: Electrophoresis agarose gel of plasmid pBR322 (9×10^{-5} mol·L^{-1}) in 20 mM TRIS/HCl buffer (pH = 7.4). Lanes 1 and 4*: DNA alone; lanes 2 and 5*: DNA + CTEAB; lanes 3 and 6*: DNA + {CTEAB@VitE}; lanes 7 and 10*: DNA alone + T4; lanes 8 and 11*: DNA +CTEAB + T4; lanes 9 and 12*: DNA + {CTEAB@VitE} + T4. B: Single strand break (SSB) ratio of DNA, CTEAB-DNA and {CTEAB@VitE}-DNA lipoplexes ± T4 with and without irradiation.*

The same behavior is observed for the {CTEAB@VitE}-DNA lipoplex. Without irradiation and after T4 treatment, no CPD are revealed (lane 9) and with irradiation and T4 treatment, the SSB ratio corresponds to addition of native abasic site level and photooxydative damage due to the irradiation (lane 12*). Thus, no significant CPD formation is shown in our experimental conditions in presence of the {CTEAB@VitE} nanoemulsion and under UVA irradiation.

Three specific scavengers were also used to understand the mechanism of the DNA photodamage by the {CTEAB@VitE} nanoemulsion. The sodium azide (NaN_3) reveals the role of the singlet oxygen in the DNA photodamage by quenching it, D_2O also by increasing the singlet oxygen lifetime and the *tert*-Butanol (^{t}BuOH) shows the implication of the hydroxyl radical species by quenching them (Fig. 9). In a previous paper,[11] it was shown that singlet oxygen was responsible for the oxidative damage in CTEAB-DNA complex. For the {CTEAB@VitE}-DNA lipoplex under UVA irradiation and with NaN_3 (lane 11*), the SSB ratio observed decreases dramatically, compared to {CTEAB@VitE}-DNA lipoplex alone (lane 10*) and until to be equal to the one for DNA alone (lane 8*). It means that the singlet oxygen is again involved on the photooxydation of the plasmid DNA by the {CTEAB@VitE} nanoemulsion. D_2O was also used to bear out the formation of singlet oxygen and its involvement on the photodegradation process. On lane 13* and Fig. 9B, a slight increase of the SSB ratio is observed for the sample on D_2O. By means of *tert*-Butanol, the involvement of hydroxyl radical species can be shown. In presence of *tert*-Butanol, the SSB ratio stays equivalent to the SSB ratio for the {CTEAB@VitE}-DNA lipoplex alone. The hydroxyl radical species are not involved on the oxidative damage of the plasmid DNA.

Consequently, the singlet oxygen is the major responsible for the direct UVA photooxydation of DNA on the {CTEAB@VitE}-DNA lipoplex. The mechanism of this process is a type II mechanism by triplet triplet energy transfer from the {CTEAB@VitE}-DNA lipoplex to the ground state of the molecular oxygen leading to the formation of the reactive singlet oxygen.

This study hightlights the role of the vitamin E as a pro-oxidant species on the {CTEAB@VitE}-DNA lipoplex by favoring the direct UVA photooxydation of the DNA duplex.

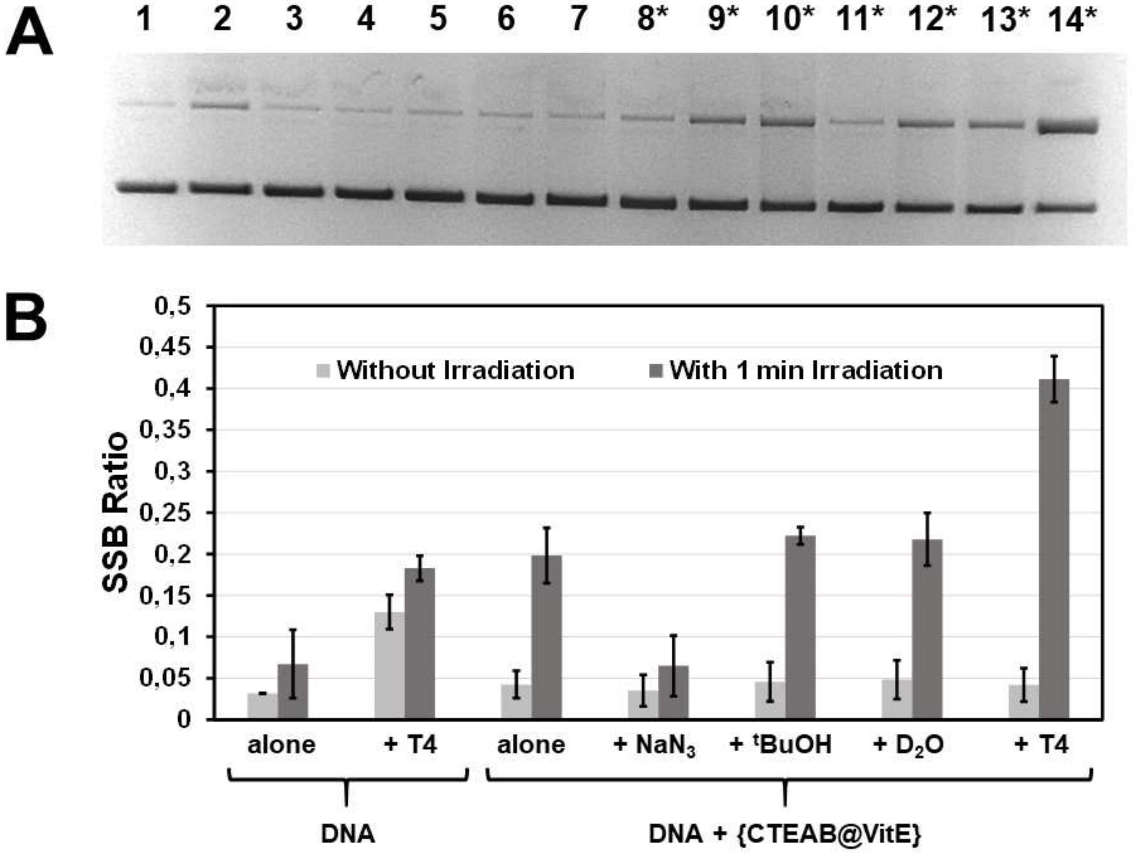

Fig. 9. *DNA cleavage for 1 min of irradiation at λ ≥ 335nm and 20°C with {CTEAB@VitE} and* NaN_3 *(*200×10^{-3} *mol·L*$^{-1}$*),* $^{t}BuOH$ *(4% v/v), in* D_2O *(80% v/v) or phage T4 endonuclease V treatment (T4) (* indicates the irradiated samples). A: Electrophoresis agarose gel of plasmid pBR322 (*9×10^{-5} *mol·L*$^{-1}$*) in 20 mM TRIS/HCl buffer (pH = 7.4). Lanes 1 and 8*: DNA alone; lanes 2 and 9*: DNA + T4; lanes 3 and 10*: DNA + {CTEAB@VitE}; lanes 4 and 11*: DNA + {CTEAB@VitE} +* NaN_3*; lanes 5 and 12*: DNA + {CTEAB@VitE} +* $^{t}BuOH$*; lanes 6 and 13*: DNA + {CTEAB@VitE} in* D_2O*; lanes 7 and 14*: DNA + {CTEAB@VitE} + T4. B: Single strand break (SSB) ratio*

of + {CTEAB@VitE}-DNA lipoplex ± NaN_3, ^tBuOH, D_2O or T4 with and without irradiation.

4. Conclusion

Various studies raise the question of the stability of Vitamin E in nanoemulsion-type systems under UVA radiation. In this work, the photosensitization of singlet oxygen by Vitamin E into self-assembled systems under UVA was studied. The cationic surfactant CTEAB has shown to be an efficient complexing agent to DNA. CTEAB surfactant was then used to form a Vitamin E-containing nanoemulsion that could interact with DNA. The self-organization properties of the CTEAB and vitamin E were studied by different physico-chemical characterizations (tensiometry, pyrene fluorimetry, and scattering experiments). The overall description of the system leads a complex fluid composed of different aggregates ranging from CTEAB micelles to a fractal network of large oil Vitamin E droplets. The study of the interactions between CTEAB-Vitamin E and plasmid DNA highlighted the gradual DNA compaction followed by gradual DNA decompaction for increasing CTEAB-Vitamin E amounts. Vitamin E seems to promote DNA decompaction.

Formulated CTEAB-vitaminE-DNA lipoplex were irradiated under UVA light. Presence of vitamin E generates a significant enhancement of the DNA photodamage. The mechanistic interpretation of the results has been highlighted by the presence of peculiar scavengers. It reveals that the singlet oxygen is responsible of the direct UVA photooxydation of DNA on the CTEAB-Vitamin E-DNA lipoplex. This study underlines the role of vitamin E as a pro-oxydant species by favoring the UVA DNA photooxydation. From a safety point of view, a warning is necessary regarding the topical pharmaceutical or cosmetic applications of such a formulation.

Acknowledgements

This work benefited from the use of the SasView application, originally developed under NSF award DMR-0520547. SasView contains code developed with funding from the European Union's Horizon 2020 research and innovation program under the SINE2020 project, grant agreement No 654000.

The research federation FERMAT (Université de Toulouse, France) is acknowledged for providing access to the Xeuss 2.0 SAXS instrument (Xenocs) through the CPER I-MATECBIO 2015-2020 grant funded by the Région Occitanie and Toulouse Métropole, and Dr. P. Roblin from the Laboratoire de Génie Chimique de Toulouse is thanked for technical support in SAXS measurements.

References

(1) Drach, M.; Narkiewicz-Michałek, J.; Sienkiewicz, A.; Szymula, M.; Bravo-Díaz, C. Antioxidative Properties of Vitamins C and E in Micellar Systems and in Microemulsions. *Colloids Surfaces A Physicochem. Eng. Asp.* **2011**, *379* (1–3), 79–85. https://doi.org/10.1016/j.colsurfa.2010.11.073.

(2) Galli, F.; Azzi, A.; Birringer, M.; Cook-Mills, J. M.; Eggersdorfer, M.; Frank, J.; Cruciani, G.; Lorkowski, S.; Özer, N. K. Vitamin E: Emerging Aspects and New Directions. *Free Radic. Biol. Med.* **2017**, *102*, 16–36. https://doi.org/10.1016/j.freeradbiomed.2016.09.017.

(3) Godic, A.; Poljšak, B.; Adamic, M.; Dahmane, R. The Role of Antioxidants in Skin Cancer Prevention and Treatment. *Oxid. Med. Cell. Longev.* **2014**, *2014*, 1–6. https://doi.org/10.1155/2014/860479.

(4) Praça, F. G.; Viegas, J. S. R.; Peh, H. Y.; Garbin, T. N.; Medina, W. S. G.; Bentley, M. V. L. B. Microemulsion Co-Delivering Vitamin A and Vitamin E as a New Platform for Topical Treatment of Acute Skin Inflammation. *Mater. Sci. Eng. C* **2020**, *110*, 110639. https://doi.org/10.1016/j.msec.2020.110639.

(5) Dad, S.; Bisby, R. H.; Clark, I. P.; Parker, A. W. Formation of Singlet Oxygen from Solutions of Vitamin E. *Free Radic. Res.* **2006**, *40* (3), 333–338. https://doi.org/10.1080/10715760500491174.Formation.

(6) Knak, A.; Regensburger, J.; Maisch, T.; Bäumler, W. Exposure of Vitamins to UVB and UVA Radiation Generates Singlet Oxygen. *Photochem. Photobiol. Sci.* **2014**, *13* (5), 820–829. https://doi.org/10.1039/C3PP50413A.

(7) Nocentini, S.; Guggiari, M.; Rouillard, D.; Surgis, S. Exacerbating Effect of Vitamin E Supplementation on DNA Damage Induced in Cultured Human Normal Fibroblasts by UVA Radiation¶. *Photochem. Photobiol.* **2001**, *73* (4),

370. https://doi.org/10.1562/0031-8655(2001)073<0370:EEOVES>2.0.CO;2.

(8) Cieśla, J.; Koczańska, M.; Narkiewicz-Michałek, J.; Szymula, M.; Bieganowski, A. Effect of α-Tocopherol on the Properties of Microemulsions Stabilized by the Ionic Surfactants. *J. Mol. Liq.* **2017**, *236*, 117–123. https://doi.org/10.1016/j.molliq.2017.04.015.

(9) McClements, D. J. Nanoemulsions versus Microemulsions: Terminology, Differences, and Similarities. *Soft Matter* **2012**, *8* (6), 1719–1729. https://doi.org/10.1039/C2SM06903B.

(10) Garbin, T. N.; Praca, F. G.; Da Silva, J. M.; Bentley, M. V. L. B.; Medina, W. S. G. Formulation, Physicochemical Characterization and in Vitro Evaluation of Water-in-Oil Microemulsion Containing Vitamin E for Topical Application. *World J. Pharm. Pharm. Sci.* **2018**, *7* (10), 38–51. https://doi.org/10.20959/wjpps201810-12412.

(11) Teychené, J.; Didacus-Prins, D.; Chouini-Lalanne, N.; Sartor, V.; Déjugnat, C. Formulation Induces Direct DNA UVA Photooxidation. Part I. Role of the Formulating Cationic Surfactant. *J. Mol. Liq.* **2019**, *295*, 111712. https://doi.org/10.1016/j.molliq.2019.111712.

(12) Bangham, A. D.; De Gier, J.; Greville, G. D. Osmotic Properties and Water Permeability of Phospholipid Liquid Crystals. *Chem. Phys. Lipids* **1967**, *1* (3), 225–246.

(13) Laouini, A.; Jaafar-Maalej, C.; Limayem-Blouza, I.; Sfar, S.; Charcosset, C.; Fessi, H. Preparation, Characterization and Applications of Liposomes: State of the Art. *J. Colloid Sci. Biotechnol.* **2012**, *1* (2), 147–168. https://doi.org/10.1166/jcsb.2012.1020.

(14) Block, I. D.; Scheffold, F. Modulated 3D Cross-Correlation Light Scattering:

Improving Turbid Sample Characterization. *Rev. Sci. Instrum.* **2010**, *81* (12), 123107. https://doi.org/10.1063/1.3518961.

(15) Ciulla, T. A.; Van Camp, J. R.; Rosenfeld, E.; Kochevar, I. E. PHOTOSENSITIZATION OF SINGLE-STRAND BREAKS IN PBR322 DNA BY ROSE BENGAL. *Photochem. Photobiol.* **1989**, *49* (3), 293–298.

(16) Aguiar, J.; Carpena, P.; Molina-Bolívar, J. A.; Carnero Ruiz, C. On the Determination of the Critical Micelle Concentration by the Pyrene 1:3 Ratio Method. *J. Colloid Interface Sci.* **2003**, *258* (1), 116–122. https://doi.org/10.1016/S0021-9797(02)00082-6.

(17) Chaudhuri, A.; Haldar, S.; Chattopadhyay, A. Organization and Dynamics in Micellar Structural Transition Monitored by Pyrene Fluorescence. *Biochem. Biophys. Res. Commun.* **2009**, *390* (3), 728–732. https://doi.org/10.1016/j.bbrc.2009.10.037.

(18) Dahesh, M.; Banc, A.; Duri, A.; Morel, M.-H.; Ramos, L. Polymeric Assembly of Gluten Proteins in an Aqueous Ethanol Solvent. *J. Phys. Chem. B* **2014**, *118* (38), 11065–11076. https://doi.org/10.1021/jp5047134.

(19) Dubois-Violette, E.; de Gennes, P.-G. Quasi-Elastic Scattering by Dilute, Ideal, Polymer Solutions: II. Effects of Hydrodynamic Interactions. *Phys. Phys. Fiz. Phys. физика* **1967**, *3* (4), 181–198. https://doi.org/10.1103/physicsphysiquefizika.3.181.

(20) Wu, C.; Zhou, S. Internal Motions of Both Poly(N -Isopropylacrylamide) Linear Chains and Spherical Microgel Particles in Water. *Macromolecules* **1996**, *29* (5), 1574–1578. https://doi.org/10.1021/ma950677k.

(21) Trappe, V.; Bauer, J.; Weissmüller, M.; Burchard, W. Angular Dependence in Static and Dynamic Light Scattering from Randomly Branched Systems.

Macromolecules **1997**, *30* (8), 2365–2372. https://doi.org/10.1021/ma961728w.

(22) Boyko, V.; Richter, S.; Burchard, W.; Arndt, K. F. Chain Dynamics in Microgels: Poly(N-Vinylcaprolactam-Co-N-Vinylpyrrolidone) Microgels as Examples. *Langmuir* **2007**, *23* (2), 776–784. https://doi.org/10.1021/la062181+.

(23) Helgeson, M. E.; Gao, Y.; Moran, S. E.; Lee, J.; Godfrin, M.; Tripathi, A.; Bose, A.; Doyle, P. S. Homogeneous Percolation versus Arrested Phase Separation in Attractively-Driven Nanoemulsion Colloidal Gels. *Soft Matter* **2014**, *10* (17), 3122. https://doi.org/10.1039/c3sm52951g.

(24) Lin, M. Y.; Lindsay, H. M.; Weitz, D. A.; Ball, R. C.; Klein, R.; Meakin, P. Universal Reaction-Limited Colloid Aggregation. *Phys. Rev. A* **1990**, *41* (4), 2005–2020. https://doi.org/10.1103/PhysRevA.41.2005.

(25) Javid, N.; Vogtt, K.; Roy, S.; Hirst, A. R.; Hoell, A.; Hamley, I. W.; Ulijn, R. V.; Sefcik, J. Supramolecular Structures of Enzyme Clusters. *J. Phys. Chem. Lett.* **2011**, *2* (12), 1395–1399. https://doi.org/10.1021/jz200446j.

(26) Lozsan, A. Salt-Induced Fast Aggregation of Nano-Emulsions: Structural and Kinetic Scaling. *Colloid Polym. Sci.* **2012**, *290* (15), 1561–1566. https://doi.org/10.1007/s00396-012-2680-4.

(27) Helgeson, M. E. Colloidal Behavior of Nanoemulsions: Interactions, Structure, and Rheology. *Curr. Opin. Colloid Interface Sci.* **2016**, *25*, 39–50. https://doi.org/10.1016/j.cocis.2016.06.006.

(28) Zhu, D.; Evans, R. K.; August, R. V; Final, I.; January, F. Molecular Mechanism and Thermodynamics Study of Plasmid DNA and Cationic Surfactants Interactions. **2006**, 3735–3743.

(29) Jumbri, K.; M.B.A. Rahman, E. Abdulmalek, E.; AHmad, H.; Micaelo, N. M. An Insight into Structure and Stability of DNA in and Experimental Studies. *Phys.*

Chem. Chem. Phys. **2014**, *16*, 14036–14046.

(30) Xu, L.; Feng, L.; Hao, J.; Dong, S. Compaction and Decompaction of DNA Dominated by the Competition between Counterions and DNA Associating with Cationic Aggregates. *Colloids Surfaces B Biointerfaces* **2015**, *134*, 105–112. https://doi.org/10.1016/j.colsurfb.2015.06.038.

(31) Feng, L.; Xu, L.; Hao, J.; Dong, S. Controlled Compaction and Decompaction of DNA by Zwitterionic Surfactants. *Colloids Surfaces A Physicochem. Eng. Asp.* **2016**, *501*, 65–74. https://doi.org/10.1016/j.colsurfa.2016.04.052.

(32) Li, X.; Sun, D.; Chen, Y.; Wang, K.; He, Q.; Wang, G. Studying Compaction-Decompaction of DNA Molecules Induced by Surfactants. *Biochem. Biophys. Res. Commun.* **2018**, *495* (4), 2559–2565. https://doi.org/10.1016/j.bbrc.2017.12.151.

Declaration of interests

▯ The authors declare that they have no known competing financial interests or personal relationships that could have appeared to influence the work reported in this paper.

☐The authors declare the following financial interests/personal relationships which may be considered as potential competing interests:

Supporting information for:

Formulation induces Direct DNA UV-A photooxidation. Part II. Pro-oxidant effect of formulated Vitamin E *via* generation of singlet oxygen

Johanne Teychené, Dalina Didacus-Prins, Nadia Chouini-Lalanne, Christophe Déjugnat*, Valérie Sartor*

1. Multi-angle dynamic light scattering (MADLS) 2
2. Multi-angle static light scattering (MASLS) 6
3. Light scattering of concentrated samples 8
4. Analysis of small angle X-ray scattering data (SAXS) 9
5. References 9

1. Multi-angle dynamic light scattering (MADLS)

In MADLS the measured autocorrelation function $g^{(2)}(q,\tau)$ of the scattered intensity $I(q,t)$ normalized over time is expressed as (1):

$$g^{(2)}(q,\tau) = \frac{\langle I(q,t)I(q,t+\tau)\rangle}{\langle I(q,t)\rangle^2} \tag{1}$$

It affords the correlation function of the electric field $g^{(1)}(q,\tau)$ using the Siegert relationship (2):

$$g^{(2)}(q,\tau) = 1 + \beta\left|g^{(1)}(q,\tau)\right|^2 \qquad \beta \leq 1 \tag{2}$$

In the ideal case of monodisperse spherical particles under Brownian motion, the autocorrelation function decays exponentially over time (3):

$$g^{(1)}(q,\tau) = \mathrm{e}^{-\Gamma\tau} \tag{3}$$

where $\Gamma = D_0 q^2$ is the decay rate and D_0 is the translational diffusion coefficient of the particles. Real situations are more complex and different algorithms can afford the decay rate from $g^{(1)}(q,\tau)$, among them Cumulant, non-negatively constrained least squares (NNLS), and CONTIN analysis. For this purpose, we used a home-made software (namely MULTI-STORMS, written and compiled with MATLAB® by Dr. C. Mingotaud). It offers the choice in the methods used to analyze the correlograms mathematical adjustments are performed using different algorithms based on the shape and the scattering properties of the particles to be analyzed.

The hydrodynamic radius of equivalent sphere (R_h) is then obtained by the Stokes-Einstein relationship (4):

$$R_h = \frac{kT}{6\pi\eta D_0} \tag{4}$$

where k is the Boltzmann constant, T the absolute temperature, and η the solvent viscosity.

Experimentally, multiple scattering was observed when measuring the {CTEAB@VitE} system (slightly opalescent) and its dilutions. The 3D cross-correlation configuration was then used to eliminate the multiple scattering contribution.[1] The experimental autocorrelation functions measured on {CTEAB@VitE} are shown in Figure S1. The curves were well fitted with a 2nd order Cumulant analysis[2] (5):

$$g^2(\tau) = B + \beta \cdot e^{-2\bar{\Gamma}\tau} \cdot \left(1 + \frac{\mu_2}{2!}\tau^2 - \frac{\mu_3}{3!}\tau^3 + \cdots\right)^2 \tag{5}$$

where B is the background value, β the amplitude of the autocorrelation function, $\bar{\Gamma}$ the mean value of the decay rates and μ_n the n^th^ moment of the distribution function of decay rates, $f(\Gamma)$. This analysis provided the intensity-weighted decay rates Γ, that did not vary linearly with respect to q^2. It indicated several contributions in the overall apparent diffusion coefficient D_{app} (translations, internal motions such as rotations, etc.).

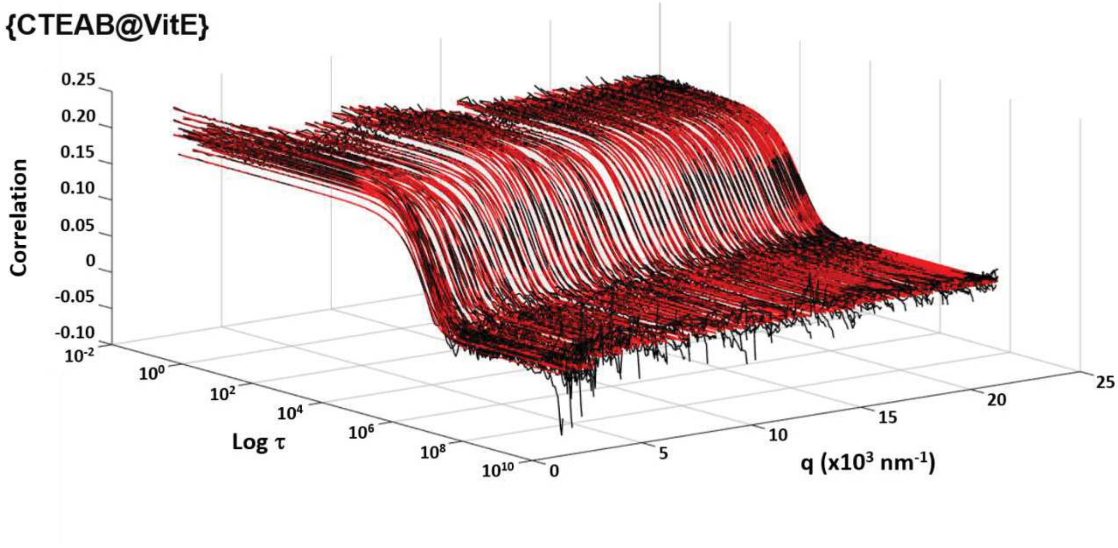

Figure S1. *Auto-correlation functions obtained from MADLS measurements of the {CTEAB@VitE} system (black curves) and the corresponding fits using a second-order Cumulant analysis (red curves).*

Similar measurements were performed in the same conditions on {CTEAB@VitE} samples after filtrations at 450 nm and 200 nm. Correlograms were also well adjusted with a 2nd order Cumulant analysis. Measurements and analysis are shown in Figures S2 and S3 (filtration at 450 nm) and in Figures S4 and S5 (filtration at 200 nm).

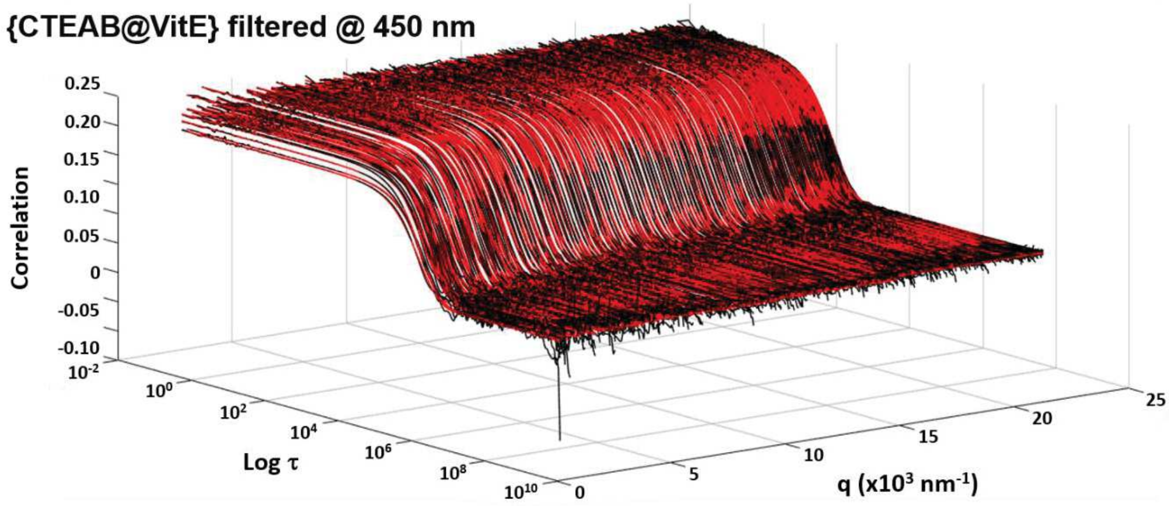

Figure S2. *Auto-correlation functions obtained from MADLS measurements of {CTEAB@VitE} filtered at 450 nm (black curves) and the corresponding fits using a second-order Cumulant analysis (red curves).*

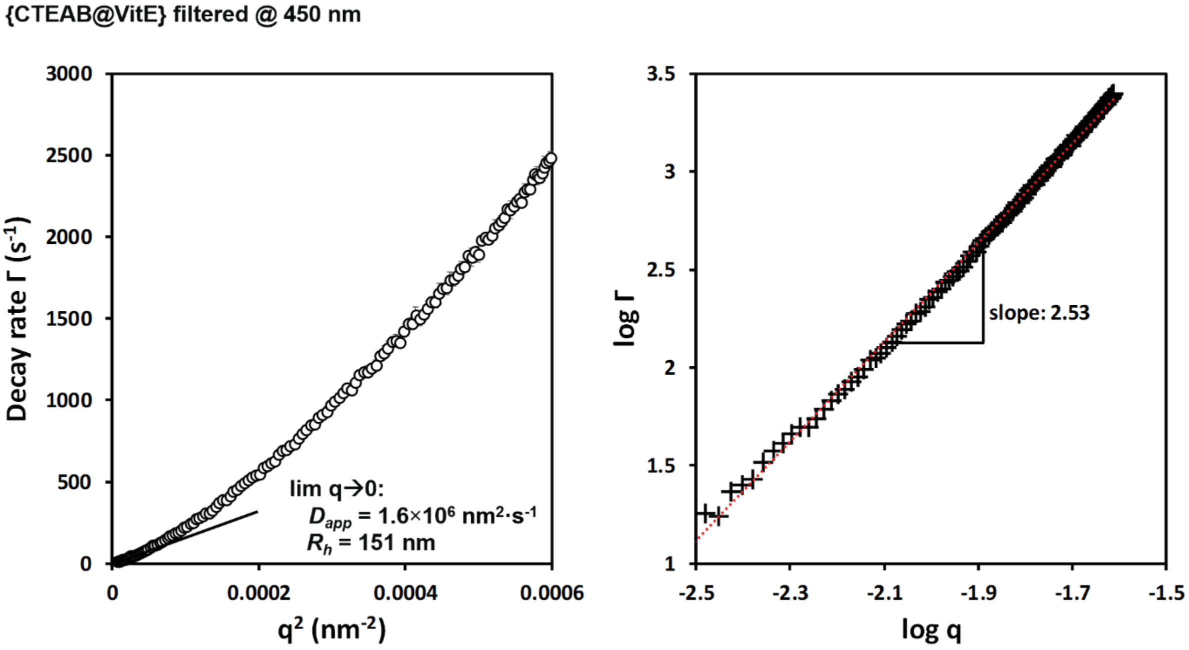

Figure S3. *(left): decay rate Γ (s^{-1}) as determined from a 2nd order Cumulant analysis, plotted as a function of q^2 from MADLS measurements of {CTEAB@VitE} filtered at 450 nm; open symbols are the experimental data and the line is the linear fit at very low q values. (right): plot of log Γ as a function of log q showing a linear dependence.*

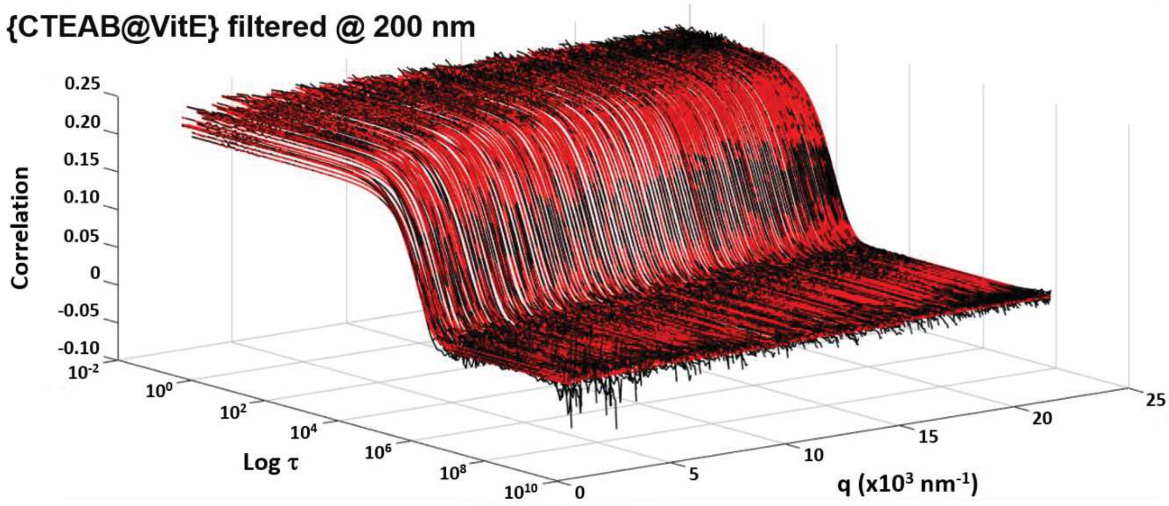

Figure S4. *Auto-correlation functions obtained from MADLS measurements of {CTEAB@VitE} filtered at 200 nm (black curves) and the corresponding fits using a second-order Cumulant analysis (red curves).*

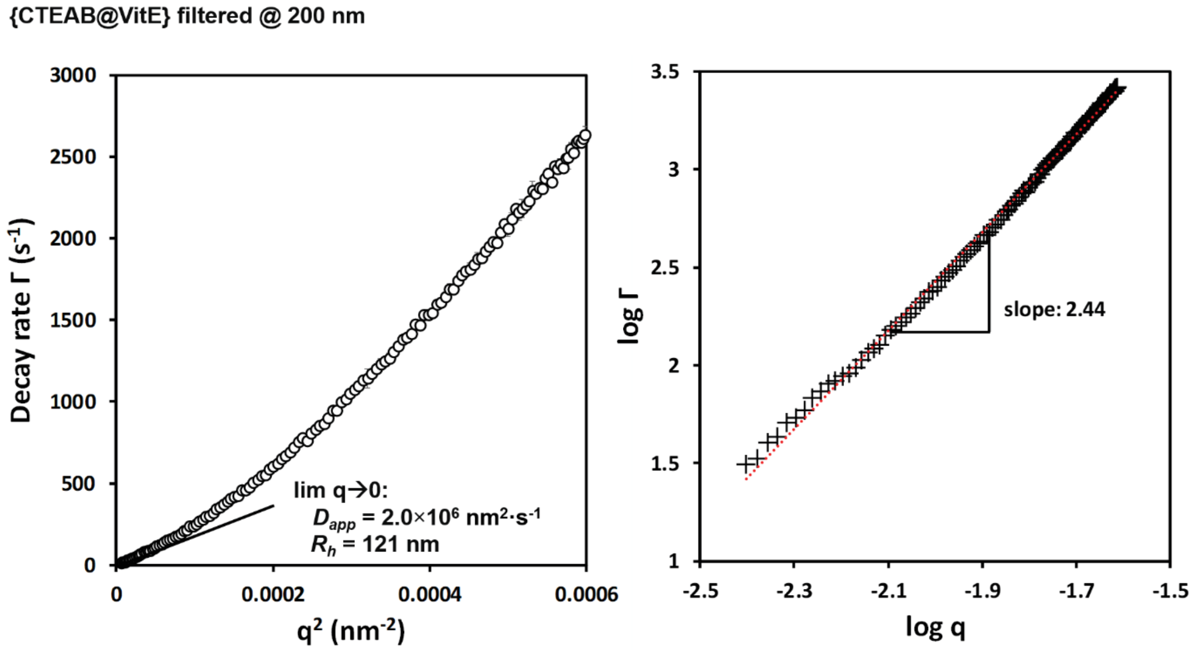

Figure S5. *(left): decay rate Γ (s^{-1}) as determined from a 2^{nd} order Cumulant analysis, plotted as a function of q^2 from MADLS measurements of {CTEAB@VitE} filtered at 200 nm; open symbols are the experimental data and the line is the linear fit at very low q values. (right): plot of log Γ as a function of log q showing a linear dependence.*

2. Multi-angle static light scattering (MASLS)

In MASLS experiments, the excess of scattered intensity with respect to the solvent is converted into absolute intensity (Rayleigh ratio R_θ, in cm^{-1}) using toluene as a reference, for which the excess Rayleigh ratio is known ($R_{\theta,toluene}$ = 1.19×10^{-5} cm^{-1} at 660 nm)[3] as described in equation (6):

$$R_{\theta,sample} = \frac{I_{sample} - I_{solvent}}{I_{toluene}} \cdot \left(\frac{n_{solvent}}{n_{toluene}}\right)^2 \cdot R_{\theta,toluene} \tag{6}$$

where I_{sample} , $I_{solvent}$, and $I_{toluene}$ are the scattering intensities of the sample solution, the solvent, and the toluene respectively, and where $n_{solvent}$ and $n_{toluene}$ are the refractive indexes of the solvent and the toluene at 660 nm, respectively (n_{water} = 1.33 and $n_{toluene}$= 1.49 at 25 °C).

MASLS profiles were then fitted using the SasView software (version 4.2.2.) applying different models:

(i) a general, empirical Guinier-Porod fit to estimate the size and the dimensionality of scattering aggregates and defined as (7-9):[4]

$$I(q) = \begin{cases} \dfrac{G}{q^s} \cdot exp\left\{\dfrac{-q^2R_g^2}{3-s}\right\} & q \le q_1 \\ \dfrac{D}{q^d} & q \ge q_1 \end{cases} \tag{7}$$

$$q_1 = \frac{1}{R_g} \cdot \left[\frac{(d-s)(3-s)}{2}\right]^{1/2} \tag{8}$$

$$D = G \cdot exp\left\{\frac{-q_1^2R_g^2}{3-s}\right\} \cdot q_1^{(d-s)} \tag{9}$$

where *G* and *D* are the Guinier and Porod scale factors respectively, R_g the radius of gyration, *d* the Porod exponent, and *s* a parameter depending on the geometry (*s*=0 for spheres, *s*=1 for rods, *s*=2 for lamellae or platelets).

(ii) A mass fractal model using the form factor $P(q)_{sphere}$ of a sphere, and described in equations (10-12):[5]

$$I(q) = scale \cdot P(q) \cdot S(q) + background \tag{10}$$

$$P(q)_{sphere} = 9 \cdot \left[\frac{\sin(qR) - qR\cos(qR)}{(qR)^3}\right]^2 \tag{11}$$

$$S(q) = \frac{\Gamma \cdot (D_m - 1) \cdot \zeta^{D_m - 1} \cdot \sin[(D_m - 1)\tan^{-1}(q\zeta)]}{q \cdot [1 + (q\zeta)^2]^{(D_m - 1)/2}} \tag{12}$$

where R is the radius of the primary particle, D_m the mass fractal dimension, and ζ the cut-off length.

(iii) The sticky hard sphere adjustment was realized combining the form factor of a sphere $P(q)_{sphere}$ (11) and a interparticle structure factor $S(q)_{stickyHS}$ for a hard sphere fluid with a narrow attractive well and using a perturbative solution of the Percus-Yevick closure. The full description of $S(q)_{stickyHS}$ can be found in the literature.[6,7]

3. Light scattering of concentrated samples

30x {CTEAB@VitE} unfiltered

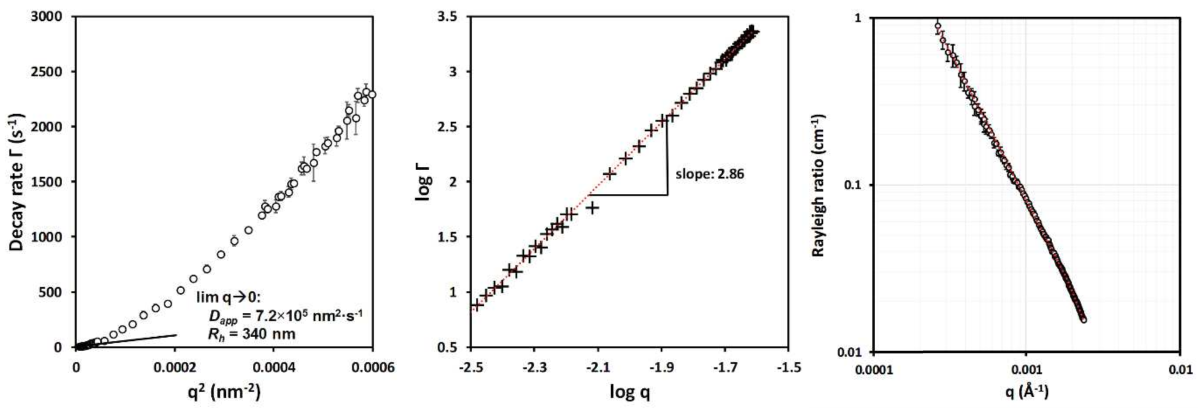

30x {CTEAB@VitE} filtered @ 450 nm

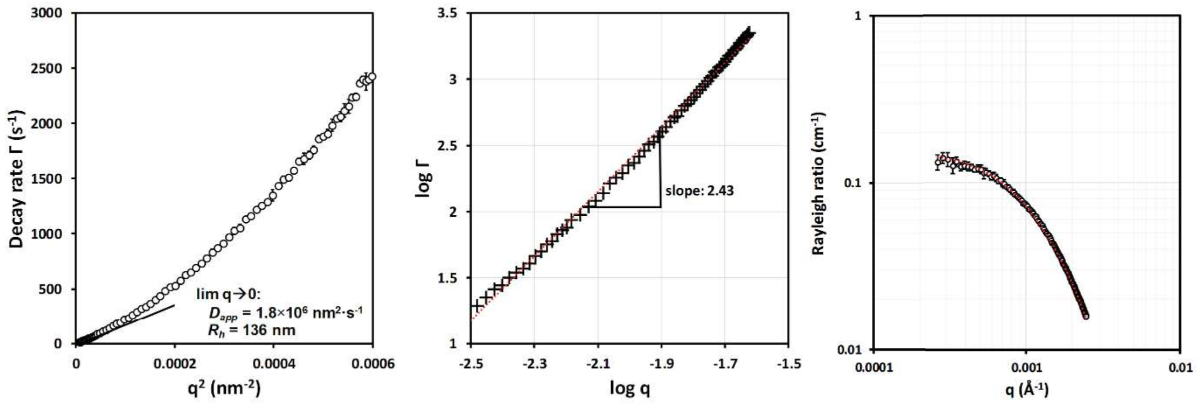

30x {CTEAB@VitE} filtered @ 200 nm

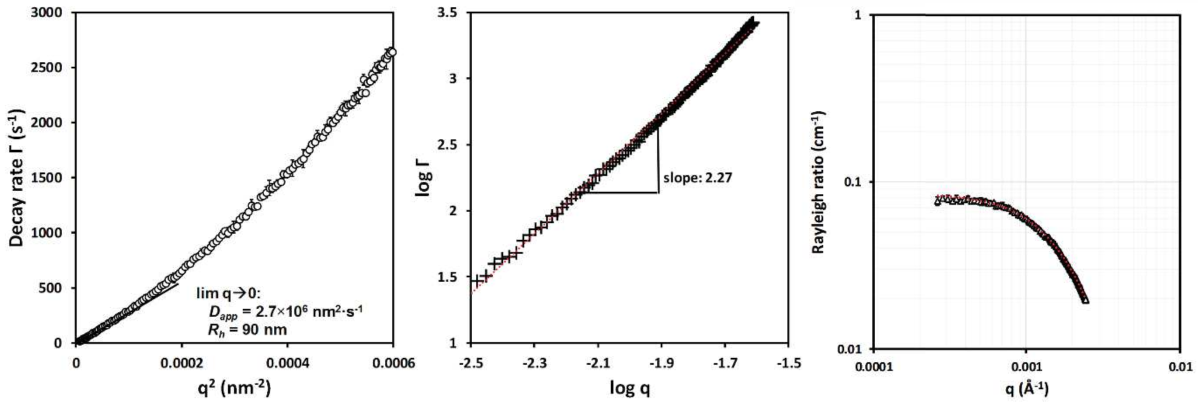

Figure S6. *(left): decay rate Γ (s^{-1}) as determined from a 2nd order Cumulant analysis, plotted vs q^2 from MADLS measurements. (center): plot of log Γ as a function of log q showing a linear dependence. (right): absolute scattered light intensities as obtained by MASLS. From top to bottom: 30x {CTEAB@VitE} unfiltered, filtered at 450 nm, filtered at 200 nm.*

4. Analysis of small angle X-ray scattering data (SAXS)

The general expression of the scattered intensity $I(q)$ is given by equation (13):

$$I(q) = \Phi \cdot \mathrm{V} \cdot (\Delta\rho)^2 \cdot P(q) \cdot S(q) \tag{13}$$

where $q = [4\pi \sin(\theta/2)]/\lambda$ is the scattering vector (θ is the scattering angle), Φ is the volume fraction of the scatterers, V is their volume and $\Delta\rho$ is their difference in scattering length density (SLD) with respect to the solvent. $P(q)$ is the scatterers' form factor and $S(q)$ is the structure factor accounting for inter-particle interactions, for which various analytical models are available.

Combining SLS and SAXS curves, the overall scattered intensity could be adjusted by a combination (14) of a fractal model and two additional sticky hard sphere models (as described above in the MASLS section):

$$I(q)_{total} = I(q)_{fractal} + I(q)_{stickyHS,1} + I(q)_{stickyHS,2} \tag{14}$$

5. References

(1) Block, I. D.; Scheffold, F. Modulated 3D Cross-Correlation Light Scattering: Improving Turbid Sample Characterization. *Rev. Sci. Instrum.* **2010**, *81* (12), 123107.

(2) Frisken, B. J. Revisiting the Method of Cumulants for the Analysis of Dynamic Light-Scattering Data. *Appl. Opt.* **2001**, *40* (24), 4087.

(3) Wu, H. Correlations between the Rayleigh Ratio and the Wavelength for Toluene and Benzene. *Chem. Phys.* **2010**, *367* (1), 44–47.

(4) Hammouda, B. A New Guinier–Porod Model. *J. Appl. Crystallogr.* **2010**, *43* (4), 716–719.

(5) Mildner, D. F. R.; Hall, P. L. Small-Angle Scattering from Porous Solids with Fractal Geometry. *J. Phys. D. Appl. Phys.* **1986**, *19* (8), 1535–1545.

(6) Menon, S. V. G.; Manohar, C.; Rao, K. S. A New Interpretation of the Sticky Hard Sphere Model. *J. Chem. Phys.* **1991**, *95* (12), 9186–9190.

(7) Gazzillo, D.; Giacometti, A. Analytic Solutions for Baxter's Model of Sticky Hard Sphere Fluids within Closures Different from the Percus–Yevick Approximation. *J. Chem. Phys.* **2004**, *120* (10), 4742–4754.